Comprehensive gene expression analysis of organoid-derived healthy human colonic epithelium and cancer cell line by stimulated with live probiotic bacteria

Akira Sen[1,2#], Atsuki Imai[1#], Kota Yanagisawa[1], Eiji Miyauchi[1], Tsukasa Oda[1], Fuki Sasaki[1], Shintaro Uchida[3], Takuhisa Okada[3], Takehiko Yokobori[4], Hiroshi Saeki[3], Toshitaka Odamaki[2], Nobuo Sasaki[1*]

1: The Laboratory for Mucosal Ecosystem Design, Institute for Molecular and Cellular Regulation, Gunma University, Maebashi, Gunma 371-8512, Japan.
2: Next Generation Science Institute, Morinaga Milk Industry Co Ltd, Zama, Kanagawa 228-8583, Japan
3: Division of Gastroenterological Surgery, Department of General Surgical Science, Gunma University, Graduate School of Medicine, Maebashi, Gunma 371-8512, Japan.
4: Initiative for Advanced Research, Gunma University, Maebashi, Gunma 371-8512, Japan.
#: These authors contributed equally to this work.
*: Correspondence: nosasaki@gunma-u.ac.jp

Abstract

The large intestine has a dense milieu of indigenous bacteria, generating a complex ecosystem with crosstalk between individual bacteria and host cells. *In vitro* host cell modeling and bacterial interactions at the anaerobic interphase have elucidated the crosstalk molecular basis. Although classical cell lines derived from patients with colorectal cancer including Caco-2 cells are used, whether they adequately mimic normal colonic epithelial physiology is unclear. To address this, we performed transcriptome profiling of Caco-2 and Monolayer cells derived from healthy Human Colonic Organoid (MHCO) cultured hemi-anaerobically. Coculture with the anaerobic gut bacteria, *Bifidobacterium longum* subsp. *longum* differentiated the probiotic effects of test cells from those of physiologically normal intestinal and colorectal cancer cells. We cataloged non- or overlapping gene signatures where gene profiles of Caco-2 cells represented absorptive cells in the small intestinal epithelium, and MHCO cells showed complete colonic epithelium signature, including stem/progenitor, goblet, and enteroendocrine cells colonocytes. Characteristic gene expression changes related to lipid metabolism, inflammation, and cell-cell adhesion were observed in cocultured live *Bifidobacterium*

longum and Caco-2 or MHCO cells. *B. longum*-stimulated MHCO cells exhibited barrier-enhancing characteristics, as demonstrated in clinical trials. Our data represent a valuable resource for understanding gut microbe and host cell communication.

Keywords

Colon cancer cells, Colonic epithelium, gene expression, gut microbiome, probiotic bacteria, transcriptome profiling

Introduction

The large intestine, also known as the colon, is a crucial component of the human digestive system with a wide range of physiological functions vital for maintaining overall health[1]. One of the primary physiological functions of the colon is the absorption of water and electrolytes from residual undigested food materials entering the colon from the small intestine[2]. The content of the partially digested chyme that passes through the colon is concentrated through water absorption, an essential process that maintains body fluid balance and prevents dehydration.

Additionally, the colon hosts a diverse community of beneficial bacteria, known as the gut microbiota, which contribute significantly to human health[3]. These microorganisms aid in fermenting undigested carbohydrates and breaking down certain substances to produce metabolites, gasses, and vitamins[4]. The gut microbiota plays a crucial role in bolstering the immune system, protecting against harmful pathogens and maintaining the intestinal lining integrity[5]. The role of microorganisms in maintaining homeostasis and influencing various aspects of human physiology has spurred research into probiotics development.

Probiotics are live microorganisms that confer health benefits when consumed in adequate quantities, and they have emerged as a promising strategy for improving human health and well-being[6]. To promote research and development of probiotics, the physiological functions of microorganisms and their effects on the host need to be investigated [7]. However, details of the fundamental molecular mechanisms underlying host cell-bacteria interactions remain largely unknown. Recent improvements in next-generation sequencing and mass spectrometry technologies have increased interest in the trans-omics analysis of gut microbiota. However, the results only provide a correlation between changes in microorganisms and their traits and do not allow direct causal inference. Therefore, *in vitro* models are required to elucidate the detailed

mechanisms of microbe-host cell interactions. However, existing models do not assess the response of normal human intestinal epithelial cells because of the difference in oxygen demands between gut bacteria (most bacteria living in the colon are anaerobes) and host cells (propagate under normoxia).

To overcome this shortcoming, researchers including our group, have developed a state-of-the-art coculture system of human colonic epithelium with highly oxygen-sensitive gut bacteria[8-12]. Colonic epithelial cells were cultured using a two-dimensional (2D) design on the Boyden chamber to establish the coculture system. Immortalized cell lines derived from human colorectal cancer tissue, such as Caco-2 cells, are commonly used to analyze gut bacteria and their metabolites[13]. Although the molecular basis is still unclear, the morphological and biochemical properties of Caco-2 cells are known to spontaneously transform, converting them into a small intestine-like epithelium following prolonged culture under confluent 2D layer conditions[14]. Consequently, Caco-2 cell monolayers have been extensively used as *in vitro* models of the small intestine to characterize certain aspects of nutrient uptake [15].

Most probiotic bacteria, such as *Akkermansia* and *Bifidobacterium* species, reside and function in the colon rather than the small intestine[16]. Thus, colonic epithelium must be used in analyzing the role of microbes inhabiting the colon. Recently, normal colonic epithelial cells were stably cultured for extended periods using three-dimensional (3D) mouse and human organoid culture methods[17, 18]. Self-renewing 2D Monolayer cultured colonic epithelium cells derived from healthy Human Colonic Organoids (MHCO) are also a physiologically relevant model[10, 19]. Moreover, primary cultured intestinal epithelial cells derived from organoids are increasingly used to study intestinal microbes.

In this study, we investigated the feasibility of using organoid-based normal human epithelium instead of Caco-2 cells in an intestinal hemi-anaerobic coculture system (iHACS)[10] containing the probiotic bacteria, *Bifidobacterium longum*. This system was established to address the limitation of currently available *in vitro* coculture systems of representative human and microbial cells. We conducted a detailed molecular analysis of the differential effects on cell physiology induced by coculture experiments with Caco-2 cells and normal colonic epithelium. By stimulating a colorectal cancer-derived cell line or normal colonic epithelium with bacteria, we aimed to generate an expression profile for the stratification of probiotic responses.

Results

Characterization of Caco-2 and colonic organoid-derived monolayer

We performed RNA-sequencing (RNA-seq) analysis to decipher the complete genetic information of the intestinal epithelium cultured using iHACS and compared two *in vitro* cell culture models of Caco-2 and 2D cultured normal colonic epithelium derived from MHCO. To collect RNA samples for transcriptome analysis, we first aligned the culture conditions of the Caco-2 and MHCO cells (Fig. 1A). To collect RNA samples for transcriptome analysis, we first align the culture conditions of Caco-2 and MHCO cells (Fig. 1A). Caco-2 was found to be able to grow in the organoid-conditioned medium, which is devoid of serum completely, so after 17 days of culture under sufficiently confluent conditions in fetal bovine serum-based DMEM Cell Culture Medium[20, 21]. The medium was changed to the organoid-conditioned medium, and RNA was recovered from cells for a further 3 days culture (Fig. 1A). Contrastingly, MHCO cells were cultured for 3 days after reaching confluence under similar conditions to those used for the Caco-2 cells (Fig. 1A). Importantly, we comparatively analyzed the gene expression in MHCO and Caco-2 cells following growth under hemi-anaerobic conditions.

Principal component analysis (PCA) of RNA-seq data from Caco-2 and MHCO cells cultured using iHACS revealed substantial differences and a clear separation of transcriptional patterns between both samples (Fig. 1B). The transcriptomes of Caco-2 and MHCO cells differed significantly, and among genes with an expression difference of > 1.5 fold change (adjusted *P*-value [*P*adj] < 0.05), we identified 4,942 and 4,824 genes that were enriched explicitly in Caco-2 and MHCO cells, respectively (Fig.1C). Furthermore, we visualized two non-overlapping classes of cell type-specific transcripts using hierarchical clustering, Caco-2 specific and MHCO cell signatures that were expressed in a mutually exclusive manner (Fig. 1D). Among the top 2,000 differentially expressed genes (DEGs), we observed several marker genes of functionally differentiated cells constituting the colonic epithelium: *Keratin 19 (KRT19*, colonocytes), *Mucin 2* (*MUC2*), *Trefoil factor 3* (*TFF3*, goblet cells), and *Chromogranin A* (*CHGA*, enteroendocrine cells) in the MHCO cell RNA-seq data (Fig. 1E, D). The stem cell marker gene, *Leucine rich repeat containing G protein-coupled receptor 5* (*LGR5*) was highly expressed in the cancer-derived cell line, whereas other markers of differentiated cells constituting the colonic epithelial tissue were highly expressed in MHCO cells (Fig. 1E). This finding was further supported by data showing that several known marker genes of the small intestine, such as *Alkaline Phosphatase, intestinal* (*ALPI*), *Alanyl*

137 *Aminopeptidase, membrane* (*ANPEP*), and *Apolipoprotein B* (*APOB*), were more highly
138 expressed in Caco-2 than they were in MHCO cells (Fig. 1D, E).
139 Next, the DEGs that differed significantly between Caco-2 and MHCO cells (Fig
140 1D) were examined using gene ontology (GO) enrichment analysis. GO analysis of the
141 genes upregulated in cultured Caco-2 cells showed enrichment of GO terms associated
142 with the Wnt signaling pathway (GO:0016055) and different transport processes,
143 including lipids (GO:0006869), organic anions (GO:0015711) and vitamins (GO:0051180,
144 Fig. 2A). The GO enrichment analysis of Caco-2 cells showed enrichment of terms
145 related to Wnt signaling pathway and lipids, organic anions, and vitamin transport
146 processes. These findings are consistent with those previously reported on the identity
147 of Caco-2 cells derived from a patient with colorectal cancer who had a mutation in the
148 *APC* gene. *APC* is a negative regulator of Wnt signaling[22] that induces the expression
149 of the target genes, *LDL Receptor Related Protein 1* (*LRP1)*[23], *Dickkopf-1* (*DKK1*)[24],
150 and *Naked cuticle 1* (*NKD1*)[25]. Additionally, GO analysis revealed a significant
151 association between the transporters of lipids (apolipoprotein family genes), organic
152 anions (*D-allose ABC transporter membrane subunit* [*ASLC*]*/solute carrier organic anion*
153 *transporter family member* [*SLCO*] family genes), and vitamins (*solute family carrier*
154 [*SLC*] *family*, *NPC1 like intracellular cholesterol transporter 1* [*NPC1L1*], *ATP binding*
155 *cassette subfamily G member 2* [*ABCG2*]) because Caco-2 cells are an extensively used
156 *in vitro* assay for nutrient abruption studies[15] (Fig. 2B).
157 In contrast, genes upregulated in MHCO cells showed a pronounced enrichment
158 of GO terms related to tissue homeostasis (GO:0001894) involved in goblet cell marker
159 genes (*MUC2* and *TFF3*) and different glycosylation processes, such as protein
160 glycosylation (GO:0006486) and macromolecular glycosylation (GO:0043413) involved
161 in the glycosylation of mucin proteins (*ST6 N-acetylgalactosaminide alpha-2,6-*
162 *sialyltransferase 1* [*ST6GALNAC1*]*, beta-1,3-galactosyltransferase 5* [*B3GALT5*]*,* and
163 *Fucosyltransferase 2* [*FUT2*]; Fig. 1E and 2A and C).
164 Furthermore, GO analysis indicated the enrichment of tissue homeostasis genes
165 (GO:0001894) exclusive to MHCO cells and involved in the mucosal immune system
166 (Fig. 2A). Immune responses to gut bacteria, Toll-like receptor 4 (*TLR4*)[26], *Aldehyde*
167 *dehydrogenase 1A1* (*ALDH1A1*)[27], and *Polymeric immunoglobulin receptor*
168 (*PIGR*)[28], were detected in MHCO cells (Fig.2C). Collectively, the presence of these
169 genes and enrichment of relevant GO confirmed that MHCO cells are more pertinent to
170 observe the physiological response of the colonic epithelium than Caco-2 cells when

171 those cells were cultured under semi-anaerobic conditions.
172
173 **Response of Caco-2 and MHCO cells to live anaerobes in the colon**
174 Caco-2 cells have been used to analyze interactions between host cells and gut
175 bacteria[29], and, therefore, we determined whether the responses of those cells to gut
176 bacteria differed from those of MHCO cells. To test the physiological effects of
177 commensal anaerobes in the colon, we cocultured Caco-2 or MHCO cells with a probiotic
178 strain of *B. longum* using iHACS. The incubation time was recently extended to allow the
179 coculture of the intestinal epithelium with anaerobic microbes[10]. Because
180 *Bifidobacterium* is generally localized in the colon, we used healthy MHCOs in this
181 study[30].
182 We confirmed that *Bifidobacterium longum* expression increased similarly in
183 Caco-2 and MHCO cells cultured with iHACS (Fig. 3A, B). After 24 h, an inoculum of 1 ×
184 10^7 colony forming units (CFU)/mL of *B. longum* increased to a median of 6.98 × 10^8 and
185 8.93 × 10^8 CFU/mL in coculture with MHCO and Caco-2 cells, respectively (P = 0.26,
186 Fig. 3B). RNA was extracted from Caco-2 and MHCO cells to assess their general
187 responses to the probiotic bacteria. In the PCA of the characterized compound classes
188 in Caco-2 and MHCO cells in the presence or absence of *B. longum* exposure (Fig. 3C),
189 the first two principal components explained 33.8% (PC1) and 17% (PC2) of the total
190 variation. PC1 indicated that MHCO cells were more distant from the clusters of Caco-2
191 cells, whereas PC2 showed the response of Caco-2 cells cocultured with *B. longum*.
192 Samples of MHCO cells alone and cocultured with *B. longum* showed a low variation in
193 each data set (Fig. 3C). Compared to the bacteria-free axenic culture, Caco-2 and
194 MHCO cells incubated with *B. longum* showed distinct transcriptomic responses, as
195 shown in the volcano plot of replicates exposed to identical conditions (Fig. 3D). After
196 filtering for adj$P$ > 0.05, the results showed that stimulation with *B. longum* affected the
197 expression of 6,127 genes in Caco-2 cells by 1.5-fold, consisting of 3,062 and 3,065
198 upregulated and downregulated genes, respectively (Fig. 3D). Similarly, 2,886 genes
199 were differentially expressed in MHCO cells, consisting of 1,407 and 1,479 upregulated
200 and downregulated genes, respectively (Fig. 3D). Additionally, the overlap of
201 upregulated DEGs between MHCO cells and Caco-2 was minimal, with only 269
202 commonly expressed genes (Fig 3E). Similarly, 296 DEGs exhibited decreased
203 expression (Fig. 3E).
204 The results of the GO analysis of genes that exhibited variations in expression in

each cell are shown in Fig. 4. We identified GO terms derived from Caco-2 or MHCO cell-specific gene expression variations following stimulation with *B. longum*. The DEGs that showed increased expression exclusively in MHCO cells were predominantly enriched in terms related to lipid metabolism, with the most enriched GO term being lipid transport (GO:0006869) (Fig. 4A). Genes downregulated in MHCO cells were associated with cell proliferation pathways such as nuclear division (GO:0000280) and chromosome segregation (GO:0007059, Fig. 4B). In Caco-2 cells, the most enriched and least downregulated GO terms were cytoplasmic translation (GO:0002181) and the Wnt signaling pathway (GO:0016055), respectively (Fig. 4C, D). Conversely, most enriched terms in the commonly upregulated genes were associated with lipopolysaccharide (GO: 0032496) and response to tumor necrosis factor (GO:0034612 and GO:0071356), whereas downregulated genes were related to double-strand break repair (GO:0006302) (Fig. 4E, F).

B. longum regulates the expression of transcription factors and genes involved in host metabolic pathway

Our analysis of the differentially induced gene expression in Caco-2 and MHCO cells following bacterial treatment showed a significant increase in the expression of genes involved in peroxisome proliferator-activated receptor (PPAR) signaling in MHCO cells (Fig. 5A). Furthermore, our transcriptome data showed that the expression of *PPARG* and *PPARA* were upregulated and downregulated in MHCO and Caco-2 cells, respectively following stimulation with *B. longum* (Fig. 5A, B). Genes of signaling pathways associated with PPARs, ketogenesis, lipid transport, cholesterol, fatty acid transporter/oxidation, adipocyte differentiation, and gluconeogenesis were upregulated in MHCO cells but not in Caco-2 cells (Fig. 5A).

To validate the upregulation of PPAR signaling in MHCO cells cocultured with *B. longum*, we focused on the expression of the PPARA and PPARG target genes. In MHCO cells coculturing with *B. longum*, *a fatty acid oxidation gene acyl-CoA oxidase 1* (*ACOX1*), a direct target gene of PPARA in the intestine[31], was elevated (Fig. 5B). *Angiopoietin like 4* (*ANGPTL4*), another identical target gene of PPARG in colonocytes[32], was also upregulated in MHCO cells (Fig. 5B). As expected, gene set enrichment analysis (GSEA) indicated that MHCO cells, but not Caco-2 cells cocultured with *B. longum* were enriched in genes related to PPAR signaling (normalized enrichment score [*NES*] = 2.06, *adj P* = 0.016 in MHCO cells, *NES* = -1.15, adj*P* = 0.53,

239 Fig. 5C). These data indicated that live *B. longum* has a potential to activate PAPR
240 signaling on normal physiological conditions of colonic epithelium.
241
242 **Differential inflammatory response to MHCO and Caco-2 cells to *B. longum***
243 **stimulation**
244 Next, we characterized the reaction of each of the cell lines to microbial stimulation by
245 determining their immune responses following stimulation and further investigated gene
246 expression profiles in the production of cytokine and chemokine molecules and their
247 regulators[33]. GSEA revealed that Caco-2 and MHCO cells stimulated by *B. longum*
248 were commonly enriched for genes associated the NF-κB signaling pathway (NES = 1.92,
249 P < 0.01, adj*P* < 0.05 in MHCO cells; NES = 2.43, *P* < 0.001, adj*P* < 0.001 in Caco-2
250 cells; Fig. 6A). To assess the responses of the Caco-2 and MHCO cells comparatively,
251 we calculated the vehicle control and *B. longum*-induced $\log_2$ fold change (FC) for each
252 gene. As expected, the responses induced by five chemokine genes (*C-C motif*
253 *chemokine ligand 20* [*CCL20*], *C-X-C motif chemokine ligand 1* [*CXCL1*], *CXCL2*, *CXCL3*,
254 and *CXCL8*) implicated in bacterial sensing[34] showed more pronounced FC values in
255 Caco-2 cells than in MHCO cells (Fig. 6B, C).
256 Moreover, bacterial inoculation of Caco-2 and MHCO cells enhanced the
257 expression of NFKB signaling target genes (*TNFAIP3*, *NFKB inhibitor alpha* [*NFKBIA*],
258 NFKB inhibitor epsilon [*NFKBIE*], NFKB inhibitor zeta [*NFKBIZ*], RELB proto-oncogene,
259 NF-κB subunit [*RELB*])[35] (Fig. 6B, C). Furthermore, *Interleukin 1A* (*IL-1A*) and *IL-1B*,
260 inflammatory cytokine genes crucial for inflammation and infection defense, were
261 significantly upregulated following coculturing of *B. longum* and MHCO cells specifically
262 [36] (Fig. 6B, C). Those results suggest that a probiotic microbe, *B. longum,* raises the
263 level of immune surveillance.
264
265 ***B. longum* upregulates intestinal barrier function in MHCO cells.**
266 We investigated the effect of Bifidobacteria on the intestinal barrier function, by
267 examining the effects on expression patterns of relevant genes. Our RNA-seq results
268 revealed substantial differences in expression patterns of genes related to the mucosal
269 barrier function between Caco-2 and MHCO cells in response to *B. longum*. The tight
270 junction-related genes, *Claudin 3* (*CLDN3*), *CLDN4,* and *Occludin* (*OCLDN*)*,* were
271 upregulated in both Caco-2 and MHCO cells following exposure to *B. longum*. In contrast,
272 other related genes, *CLDN7* and *Tight junction protein 3* (*TJP3*), were only upregulated

273 in MHCO cells, whereas *CLDN2* was upregulated in Caco-2 cells (Fig. 7A, B). Other
274 components of the adherens junction (Cadherin 1 [*CDH1*], *CDH17*, *Epithelial cell*
275 *adhesion molecule* [*EPCAM*]) or desmosomes (*Desmoglein 2* [*DSG2*] and *Dystonin*
276 [*DST*]) were linked to a set of genes that were upregulated in *B. longum*-stimulated
277 MHCO cells and conversely downregulated in Caco-2 cells (Fig. 7A, C, D). The polarity
278 of intestinal epithelial cells plays a central role in establishing the barrier function for
279 symbiotic relationships with microbiota[37]. The *B. longum*-induced expression pattern
280 of *Integrin subunit α6* (*ITGA6*), a significant factor in the epithelium and basement
281 membrane interaction, also differed between MHCO and Caco-2 cells (Fig. 7A, E).
282 To investigate whether increased gene expression induced by *B. longum* was
283 associated with improved barrier function, we measured the transepithelial electrical
284 resistance (TEER) in MHCO cells. Compared to the vehicle control, TEER was
285 significantly increased in cells cocultured with *B. longum* (Fig. 7D). We also evaluated
286 the paracellular permeability of the colonic epithelium using the Lucifer yellow (LY) flux
287 assay with the fluorescent molecule LY, which does not interact with cell components[38].
288 Consistent with the changes in TEER, LY flux was downregulated when MHCO cells
289 were cultured with *B. longum* (Fig. 7E). Overall, these results confirmed the previous
290 studies in MHCO cells with live *B. longum* in hemi-anaerobic culture conditions that
291 probiotic *Bifidobacteria* enhance intestinal barrier integrity through PPARG/STAT3
292 pathway.
293
294 **Discussion**
295 In this study, we compared gene expression data between Caco-2 and MHCO cells
296 cultured under hemi-anaerobic conditions to provide valuable datasets for investigating
297 host cells and anaerobic bacteria in the colon. We demonstrated the presence of all cell
298 types that form the colonic epithelium, including stem, goblet, and enteroendocrine cells
299 and colonocytes among the MHCO cells cultured under hemi-anaerobic conditions. In
300 contrast, the gene expression pattern of Caco-2 cells was similar to that of epithelial cells
301 of the small intestine, as shown previously[39]. Therefore, MHCO cells may be a
302 physiologically appropriate model for studying probiotic activities, including of
303 *Bifidobacterium* and *Akkermansia*, in the colon[30, 40].
304 The Caco-2 cell line generated from a patient with colorectal cancer is the most
305 commonly used in studying the physiological functions of the human intestinal epithelium.
306 These cells spontaneously transform to differentiate and form monolayers of polarized

307 cells with functions similar to those of enterocytes in the small intestine when grown
308 under confluent conditions in Boyden chambers. Consequently, Caco-2 cells have been
309 widely used to investigate the metabolism and absorption of drugs and nutrients[15, 41].
310 The intestinal environment where enterobacteria are localized is physiologically hypoxic,
311 which affects gene expression patterns through the chromatin state and metabolic
312 pathways[42].

313 Gnotobiotic mice have been the primary animal model used in previous studies
314 of the effect of microbes on hosts. Although studies using in vivo mouse models provide
315 important insights into the physiology of host-microbiome interactions, they are unable
316 to account for significant differences between mice and humans because bacteria exhibit
317 strong species specificity[43]. Conventionally, cell lines derived from patients with cancer
318 have been used to study microbial responses. In this study, healthy primary colonic
319 epithelial cells cultured as organoids and a conventional colorectal cancer-derived cell
320 line were used to examine the physiological response of the host epithelium to microbiota.
321 The gene expression patterns in the DEG analysis in our study indicated that healthy
322 human colonic epithelium derived from organoids was more robust against gut bacteria
323 than the cancer-derived Caco-2 cell line was. These results demonstrated the observed
324 low incidence of overlapping upregulated DEGs between MHCO and Caco-2 cells and
325 decreased expression of DEGs, indicating that the impact of coculturing with *B. longum*
326 on gene expression was not conserved across these two cell types.

327 Caco-2 cells have been used to assess the efficacy of probiotics and intestinal
328 bacteria in evaluating mucosal barriers and inflammatory responses. However, two
329 independent reports demonstrated the immunoreactivity of *Faecalibacterium prausnitzii*
330 (recently reclassified as *Faecalibacterium duncaniae*) in host cells using Caco-2 cells or
331 primary colonic epithelium (organoid)[12, 44]. To the best of our knowledge, this study is
332 the first to evaluate the effect of gut bacteria on Caco-2 cells and colonic organoids
333 incubated under matched culture and hemi-anaerobic conditions.

334 In this study, the expression of various inflammation-related genes was similarly
335 induced by *B. longum* in Caco-2 and organoid-derived healthy epithelial cells. However,
336 the fold-change ratio was higher in Caco-2 cells than it was in the organoid cells. This
337 probably occurred because Caco-2 cells lack goblet cells and poorly express genes such
338 as *MUC2*, which renders the barrier function of the intestinal epithelium vulnerable.
339 Moreover, the bacteria may have more readily caused inflammation in the Caco-2 cells
340 than in MHCO cells. Therefore, we focused on immune responses to characterize the

341 reaction of Caco-2 and MHCO cells to microbial stimulation because genes commonly
342 upregulated in these cell lines show pronounced enrichment of GO terms associated
343 with inflammation. The intestinal epithelium interfaces directly with the external
344 environment and acts as a constant frontline defense for the immune response[45].
345 Epithelial cells play an essential role in preventing bacterial invasion by producing
346 cytokines and chemokines that determine the nature of the immune response by
347 controlling immune cells. These facts prompted our investigation of gene expression
348 profiles in the production of immune-related molecules and their regulators, including
349 NFKB inhibitors and TNFAIP[33]. The results suggest that the probiotic microbe, *B.*
350 *longum,* raised levels of immune surveillance.

351 In addition, our GSEA results showing the enrichment of genes related to PPAR
352 signaling in bacterial-stimulated MHCO but not Caco-2 cells led us to conclude that live
353 *B. longum* has the potential to activate PAPR signaling under normal physiological
354 conditions in the colonic epithelium. These observations further confirmed that MHCO
355 cells are more pertinent for observing the physiological response of the colonic
356 epithelium than Caco-2 cells are when cultured under semi-anaerobic conditions.

357 Moreover, the results of the TEER analysis corroborated the relationship between
358 *B. longum*-induced increase in gene expression and improved barrier function in MHCO
359 cells. These observations further confirmed the findings of previous studies in MHCO
360 cells cocultured with live *B. longum* under hemi-anaerobic culture conditions, which
361 showed that probiotic *Bifidobacteria* enhanced the intestinal barrier integrity through the
362 PPARG/signal transducer and activator of transcription 3 (STAT3) pathway. Previous
363 animal and clinical studies have revealed that *Bifidobacterium*, a probiotic, positively
364 regulates the barrier function of mucosal epithelial cells[46].

365 Epithelial cells are held together by strong anchoring junctions that include tight
366 junctions, adherens junctions, and desmosomes, which are formed by transmembrane
367 adhesion proteins*[47].* The expression of *CLDN4*, a component of tight junctions, has
368 been shown to be upregulated in the colonic epithelial cells of mice administered
369 *Bifidobacteria[48].* Similarly, our investigation using human colonic organoids cocultured
370 with *B. longum* also showed the upregulation of *CLDN4*. Contrastingly, several
371 molecules related to epithelial cell junctions, such as *CLDN2*, showed conflicting
372 expression patterns in Caco-2 and MHCO cells stimulated with *B. longum*. *CLDN2* is a
373 pore-forming CLDN that permeates water and ions and has been reported to be elevated
374 in patients with inflammatory bowel disease or neonatal necrotizing enterocolitis[49-52].

375 Furthermore, we found that *CLDN7*, a tight junction-related gene, was upregulated only
376 in MHCO monolayer cells cocultured with *B. longum*. Increased *CLDN2* and decreased
377 *CLDN7* levels have previously been observed in the gastrointestinal tracts of patients
378 with ulcerative colitis[53], and *CLDN7* knockout mice develop colitis spontaneously[54].
379 In this study, to the best of our knowledge, we provide the first proof that *Bifidobacterium*
380 modulates *CLDN7* expression in the physiologically normal human colonic epithelium.
381 The polarity of intestinal epithelial cells plays a central role in establishing a
382 barrier function for symbiotic relationships with microbiota[37]. Hemidesmosomes, which
383 are composed of ITGA6T and are a significant factor in the interaction between the
384 epithelium and basement membrane, are expressed at specific junctions in the basal
385 portion of intestinal epithelial cells[55]. In addition to other factors, improvement of the
386 mucus barrier function is a known molecular mechanism in coculture systems. A novel
387 finding of this study is that more genes were altered by bacterial stimulation in Caco-2
388 cells than they were in the organoids. While both organoids and Caco-2 cells share
389 certain variable gene sets, each cell line exhibited a unique variation in the expression
390 of genes linked to inflammation and the mucosal barrier, which are well-known roles of
391 *Bifidobacterium*. However, the potential usefulness and applicability of *Bifidobacterium*
392 needs to be further investigated using appropriate *in vitro* culture systems.
393

394 **Methods**

395 **Colonic organoid culture**

396 Clinical samples for healthy human colonic organoid establishment and coculturing
397 microbes were obtained from patients at Gunma University Hospital with informed
398 consent after study approval by the ethical committees (HS2022-054). The human
399 colonic organoid was cultured as in the previous report with minor modifications[10].
400 Briefly, three-dimensional colonic organoids were maintained with Modified human
401 colonic organoid (MHCO) medium, consisting of advanced Dulbecco's modified Eagle's
402 medium (DMEM)/F12 supplemented with penicillin/streptomycin, HEPES, Glutamax, B-
403 27 Supplement (Thermo Fisher Scientific, Waltham, MA), 1 mM N-acetylcysteine
404 (Sigma-Aldrich), 50 ng/mL recombinant mouse epidermal growth factor (Thermo Fisher
405 Scientific), 100 ng/mL mouse recombinant noggin (Peprotech), 1μg/mL human
406 recombinant R-spondin1 (R&D), 100 ng/mL recombinant human insulin-like growth
407 factor-1 (BioLegend, San Diego, CA), 50 ng/mL recombinant human fibroblast growth
408 factor-basic (FGF-2) (PeproTech) and conditioned medium containing Wnt3A. The
409 human colonic organoid was derived from a nonpathological biopsy and confirmed by
410 genomic sequencing analysis that it has no driver mutations related to colorectal cancer,
411 as shown in the previous paper[2]. Organoids were passed approximately every 5-7 days
412 by physical dissociation using fire-polished Pasteur pipettes. To generate MHCO cells,
413 ThinCert culture inserts (24-well insert, 0.4 μm pore polyester membrane; Greiner bio-
414 one, Kremsmunster, Austria) were coated with 4% Matrigel diluted with advanced
415 DMEM/F12 medium and incubated at 25ºC for 30 minutes, then Matrigel solution was
416 removed. The membrane was dried in a tissue-culture hood for 15 minutes. Human
417 colonic organoids were cultured for 3 to 5 days before being used to plate into monolayer
418 culture in MHCO medium. Three-dimensional cultured organoids were treated with
419 TrypLE Express (Thermo Fisher Scientific) to dissociate into single cells. The cells were
420 resuspended to 1×10^6 cells/mL in MHCO medium containing 10 μM Y-27632 (FUJIFILM
421 Wako Pure Chemical Corporation, Osaka, Japan), and 200 uL of cell suspension was
422 added into the transwell inserts. After 1 day of monolayer culture, MHCO without Y-
423 27632 was used, and the medium was changed every 2 days. When MHCO cells were
424 cultured in the inserts, MHCO without penicillin/streptomycin was used for their
425 maintenance.

426

427 **Caco-2 cell culture**

428 The cell line Caco-2 maintained in our group was confirmed by the Cell Line
429 Authentication Service (ATCC). Caco-2 cells were maintained with the medium
430 consisting of DMEM (high glucose) with L-Glutamine and Phenol Red (FUJIFILM Wako
431 Pure Chemical Corporation) supplemented with 10% heat-treated FBS (Hyclone, Logan,
432 UT), MEM Non-Essential Amino Acids Solution (Nacalai tescue, Kyoto, Japan), and
433 penicillin/streptomycin. Caco-2 cells were passaged approximately 3-5 days before
434 reaching 80% confluency using 0.25% Trypsin-EDTA (Gibco, Waltham, MA, USA) and
435 seeded at 2-4 x10^4 cells/cm^2. 10^5 cells were seeded in transwell culture insert coated
436 Matrigel solution described above. Cells were cultured with the 10% FBS-containing
437 DMEM medium for 17 days. Before the coculture experiment, the culture medium was
438 changed to MHCO medium without antibiotics and cultured for 2 days.
439
440 **Bacterial culture**
441 *B. longum* subsp. *longum* JCM1217^T (*B. longum*) was obtained from the Riken
442 BioResource Research Center (JCM, Tokyo, Japan). This strain was cultured in modified
443 GAM broth (Nissui Pharmaceutical, Gifu, Japan) for 4 hours at 37ºC under anaerobic
444 conditions using a BACTRON300 anaerobic chamber (Sheldon Manufacturing, Inc.,
445 Cornelius, USA). The culture medium was centrifuged (8,000 x g, 1 min, 25ºC) and
446 suspended to approximately 5.0 × 10^7 CFU/mL in a deoxygenated WENRAIF medium
447 supplemented with 100mM HEPES in an anaerobic chamber. Then, 200 uL bacterial
448 suspension was added at the apical side of the transwell in an anaerobic chamber and
449 capped in butyl gum caps. Then, the basolateral side's medium was cultured in a CO2
450 incubator for 24 hours. The number of colony-forming units (CFU) on TOS propionate
451 agar (Yakult Pharmaceutical Industry, Tokyo, Japan) was used to calculate the number
452 of live *B. longum*.
453
454 **RNA isolation and sequencing**
455 Total RNA was extracted using the RNeasy Mini Kit (Qiagen) with an RNase-Free DNase
456 Set (Qiagen). Library preparation was performed using Illumina Stranded mRNA Prep
457 and IDT® for Illumina® RNA UD Indexes Set A-B Ligation (Illumina, San Diego, CA,
458 United States). The concentration and quality of the extracted RNA and adapter-tagged
459 sequence library were calculated using Agilent RNA 6000 Nano and Agilent High
460 Sensitivity DNA Kits (Agilent Technologies, Santa Clara, CA, USA), respectively.
461 Sequences were obtained using the NextSeq 1,000 system with the Illumina NextSeq

462 1000/2000 P2 Reagent kit (100 cycles) (Illumina). Read files were trimmed and mapped
463 to the human reference genome (GRCh38.p.13) using Trim Galore! (ver.0.6.4,
464 https://github.com/FelixKrueger/TrimGalore) and HISAT2 (ver.2.2.1) (Graph-Based
465 Genome Alignment and Genotyping with HISAT2 and HISAT-genotype - PMC (nih.gov))
466 with default settings[56]. Transcript assembly, GTF document merging, and transcript
467 quantification were performed using Stringtie (ver.2.2.0) (StringTie enables improved
468 reconstruction of a transcriptome from RNA-seq reads - PubMed (nih.gov))[57]. A matrix
469 of read counts mapped to genes was extracted using prepDE.py
470 (http://ccb.jhu.edu/software/stringtie/dl/prepDE.py3).
471
472 **Data analysis and visualization**
473 Normalization from read counts and identifying differentially expressed genes (DEGs)
474 were performed via iterative differential expression analysis (DESeq2) by iDEP1.1
475 software. Adjusted p-value <0.05 and $\log_2$ fold change >1.5 were defined as DEGs.
476 Statistical analysis and data visualization were performed using R (ver.4.3.2). The
477 principal component analysis (PCA) was performed using the 'prcomp' function with TPM
478 matrix in the stats package (ver.3.6.2,
479 https://www.rdocumentation.org/packages/stats/versions/3.6.2) with scaling. The
480 hierarchical clustering and plotting of the heatmap were performed by the 'Heatmap'
481 function in the ComplexHeatmap package (ver.2.18.0,
482 https://github.com/jokergoo/ComplexHeatmap). Functional enrichment analysis of DEGs
483 was performed using the 'enrichGO' function in the clusterProfiler package (ver.4.10.0,
484 https://github.com/YuLab-SMU/clusterProfiler) and GO terms with p-value <0.05 and
485 adjusted p-value <0.05 were considered significant. KEGG pathway enrichment analysis
486 was performed using the 'gseKEGG' function in the clusterProfiler package, and the
487 significantly enriched pathways were defined by nominal adjusted p-value <0.05.
488
489 **Measurement of the integrity of the cell monolayer**
490 The integrity of the cell monolayer was assessed with relative TEER value and LY assay.
491 TEER was measured by Millicell ERS-2 Voltohmmeter (Merck Millipore, USA) following
492 the manufacturer's instruction. Relative TEER was calculated by TEER value after Hemi-
493 Anerobic cultivation for 24 hours relative to their initial value (0 hours). HBSS
494 supplemented with 10mM HEPES, D-PBS(+) Preparation Reagent (Ca, Mg Solution)
495 (Nacalai tesque, Kyoto, Japan) were used as transport buffers. After washing the

monolayer with transport buffer, 300uL of Lucifer yellow solution (300uM prepared in transport buffer) and 1000uL of transport buffer were added to the apical and basolateral sides of the monolayers, respectively. The monolayers were incubated for 60 minutes in a CO2 incubator. After incubation, 200uL of apical and basolateral solution was collected in the 96-well black assay microplate, and the fluorescence was measured at an emission wavelength of 538 nm and excitation at 485 nm using Perkin Elmer Enspire 2300 Multi-mode Microplate Reader with EnSpire Workstation (version 4.13.3005.1482) n=4 biological replicates.

Acknowledgment: The authors thank the members of Gastroenterological Surgery, School of Medical Faculty of Medicine at Gunma University for human sample collection and all members of the laboratory for Mucosal Ecosystem Design for their assistance in experiments and discussion. A Wnt3a-producing cell line was a kind gift from Hans Clevers (Hubrecht Institute).

Funding: This work was supported in part by the Japan Agency for Medical Research and Development (AMED) grant (JP 23ae0121046), JST FOREST program (JPMJFR2161), Grants-in-Aid for the Japanese Society for the Promotion of Science (JSPS) KAKENHI (19H03455, 23H02713), a Grant-in-Aid for Challenging Research (Pioneering, 23K17415), the Astellas Foundation for Research on Metabolic Disorders, and the LOTTE Foundation.

Author contributions:

A.S., A.I., F.S., and T. Odamaki performed all the empirical experiments and analyzed the data. A. S., A. I., K. Y., E. M., and T. Oda. performed and analyzed the RNA-seq data. S.U., T. Okada, T.Y., and H.S. provided tissue specimens. N.S. conceived and conducted the project. A.S. and N.S. wrote the manuscript. All authors discussed the results and edited the manuscript.

Conflict of interest

A. S. and T. O. are employees of Morinaga Milk Industry Co. Ltd. The remaining authors disclose no conflicts.

529 **Figure legends**

530 **Figure 1. Comparison of gene expression profiles between human colonic**
531 **organoid-derived monolayers (MHCO) and Caco-2.**

532 **(A)** A schematic representation of the experiment. **(B)** PCA of the transcriptomes of
533 MHCO and Caco-2. Each plot represents a single transcriptome. Transcriptomes from
534 three replicates were plotted. Ellipses indicate the 95% confidence interval. **(C)**
535 Volcano plot depicting the DEGs of the transcriptomes of MHCO and Caco-2. The x-
536 and the y-axis show the $\log_2$ transformed fold change and the $-\log_{10}$ transformed
537 adjusted p-value. Red and blue dots indicate significantly upregulated genes in MHCO
538 and Caco-2 according to adjusted p-value <0.05 and $\log_2$ fold change >1.5. **(D)**
539 Heatmap depicting the top-2000 DEGs of the transcriptomes of MHCO and Caco-2
540 when sorted by adjusted p-value. **(E)** TPM values of marker genes for each gut
541 epithelial cell type. Data are presented as the mean ± Standard derivatives (SD).
542 Statistical significance was evaluated by Welch's *t*-test.

543

544 **Figure 2. GO enrichment analysis of DEGs of the transcriptomes of MHCO and**
545 **Caco-2.**

546 **(A)** Dot plot showing GO terms associated with DEGs for Caco-2 (left panel) and
547 MHCO (right panel) identified in **Figure 1D**. **(B)** TPM values of representative genes for
548 each GO term. Data are presented as the mean ± Standard derivatives (SD). Statistical
549 significance was evaluated by Welch's *t*-test.

550

551 **Figure 3. Differences in gene expression change among MHCO and Caco-2 after**
552 **coculturing with *B. longum*.**

553 **(A-D)** A schematic representation of the experiment. **(B)** Colony-forming units (CFU)
554 counts per milliliter of *B. longum* inoculated after 24-hour incubation with MHCO and
555 Caco-2 using iHACS. **(C)** PCA of the transcriptomes of MHCO and Caco-2 cocultured
556 with or without *B. longum*. Each plot represents a single transcriptome. Transcriptomes
557 from three replicates were plotted. Ellipses indicate the 95% confidence interval. **(D)**
558 Volcano plot depicting the upregulated and downregulated genes of Caco-2 (left panel)
559 and MHCO (right panel) after coculturing with *B. longum*. The x- and the y-axis show
560 the $\log_2$ transformed fold change and the $-\log_{10}$ transformed adjusted p-value. Red and
561 blue dots indicate significantly upregulated and downregulated genes after coculturing
562 with *B. longum* according to adjusted p-value <0.05 and $\log_2$ fold change >2. **(E)** Venn

563 diagram comparing the significantly upregulated (left panel) and downregulated genes
564 (right panel) in MHCO or Caco-2 after coculturing with *B. longum*.
565
566 **Figure 4. GO enrichment analysis of upregulated and downregulated genes in**
567 **MHCO and Caco-2 after coculturing with *B. longum*.**
568 **(A-F)** Dot plot showing GO terms associated with upregulated (**A-C**) and
569 downregulated genes (**D-F**) in MHCO (**A**, **D**), Caco-2 (**B**, **E**), and both (**C**, **F**) identified
570 in **Figure 3E**.
571
572 **Figure 5. *B. longum* regulates the PPAR signaling pathway.**
573 **(A)** Heatmap of relative expression of PPAR signaling-related genes by co-cultivation
574 of *B. longum* in Caco-2 and MHCO. Statistical significance was evaluated by a Deseq2
575 (*adjusted p-value <0.05, ** adjusted p-value <0.01, *** adjusted p-value <0.001). **(B)**
576 TPM values of representative PPAR receptor and its target genes. Data are presented
577 as the mean ± Standard derivatives (SD). Statistical significance was evaluated by
578 Welch's *t*-test. **(C)** Enrichment plot of genes in Ppar Signaling Pathway (KEGG) for
579 MHCO (left panel) and Caco-2 (right panel). Each vertical bar represents a gene, and
580 genes enriched in upregulated and downregulated after coculturing with *B. longum* are
581 at the left and right part of the graph, respectively. The normalized enrichment score
582 (NES), the p-value, and the false discovery rate (Adjusted p-value) were indicated in
583 the insert.
584
585 **Figure 6. *B. longum* regulates inflammatory response differently in MHCO and**
586 **Caco-2.**
587 **(A)** Enrichment plot of genes in Nf-Kappa B Signaling Pathway (KEGG) for MHCO (left
588 panel) and Caco-2 (right panel). **(B)** Heatmap of relative expression of inflammatory
589 response-related genes by co-cultivation of *B. longum* in Caco-2 and MHCO. Statistical
590 significance was evaluated by a Deseq2 (*adjusted p-value <0.05, ** adjusted p-value
591 <0.01, *** adjusted p-value <0.001). **(C)** TPM values of representative chemokine, NF-
592 κB related, and inflammatory cytokine genes. Data are presented as the mean ±
593 Standard derivatives (SD). Statistical significance was evaluated by Welch's *t*-test.
594
595 **Figure 7. *B. longum* regulates intestinal barrier function.**
596 **(A)** Heatmap of relative expression of cell junction-related genes by co-cultivation of *B.*

longum in Caco-2 and MHCO cells. Statistical significance was evaluated by a DESeq2 (*adjusted p-value <0.05, ** adjusted p-value <0.01, *** adjusted p-value <0.001). **(B)** TPM values of representative tight junction (upregulated in both MHCO and Caco-2 cells, specifically upregulated in MHCO), adherence junction, and hemidesmosome-related genes. Data are presented as the mean ± Standard derivatives (SD). Statistical significance was evaluated by Welch's *t*-test. **(C, D)** Relative TEER value adjusted by the initial value (**C**) and permeability of Lucifer Yellow (LY) from apical to basolateral compartment (**D**) in MHCO cocultured with *B. longum* versus vehicle control. Data are expressed as means ± SD. Statistical significance was evaluated using Welch's t-test.

607 **References**

608 [1] J.R. Turner, Intestinal mucosal barrier function in health and disease, Nat Rev Immunol, 9
609 (2009) 799-809.
610 [2] P.R. Kiela, F.K. Ghishan, Physiology of Intestinal Absorption and Secretion, Best Pract Res
611 Clin Gastroenterol, 30 (2016) 145-159.
612 [3] S.V. Lynch, O. Pedersen, The Human Intestinal Microbiome in Health and Disease, N Engl J
613 Med, 375 (2016) 2369-2379.
614 [4] I. Rowland, G. Gibson, A. Heinken, K. Scott, J. Swann, I. Thiele, K. Tuohy, Gut microbiota
615 functions: metabolism of nutrients and other food components, Eur J Nutr, 57 (2018) 1-24.
616 [5] D. Zheng, T. Liwinski, E. Elinav, Interaction between microbiota and immunity in health and
617 disease, Cell Res, 30 (2020) 492-506.
618 [6] M.E. Sanders, D.J. Merenstein, G. Reid, G.R. Gibson, R.A. Rastall, Probiotics and prebiotics
619 in intestinal health and disease: from biology to the clinic, Nat Rev Gastroenterol Hepatol, 16
620 (2019) 605-616.
621 [7] J. Plaza-Diaz, F.J. Ruiz-Ojeda, M. Gil-Campos, A. Gil, Mechanisms of Action of Probiotics,
622 Adv Nutr, 10 (2019) S49-S66.
623 [8] S. Jalili-Firoozinezhad, F.S. Gazzaniga, E.L. Calamari, D.M. Camacho, C.W. Fadel, A. Bein, B.
624 Swenor, B. Nestor, M.J. Cronce, A. Tovaglieri, O. Levy, K.E. Gregory, D.T. Breault, J.M.S. Cabral,
625 D.L. Kasper, R. Novak, D.E. Ingber, A complex human gut microbiome cultured in an anaerobic
626 intestine-on-a-chip, Nat Biomed Eng, 3 (2019) 520-531.
627 [9] R. Kim, P.J. Attayek, Y. Wang, K.L. Furtado, R. Tamayo, C.E. Sims, N.L. Allbritton, An in
628 vitro intestinal platform with a self-sustaining oxygen gradient to study the human
629 gut/microbiome interface, Biofabrication, 12 (2019) 015006.
630 [10] N. Sasaki, K. Miyamoto, K.M. Maslowski, H. Ohno, T. Kanai, T. Sato, Development of a
631 Scalable Coculture System for Gut Anaerobes and Human Colon Epithelium, Gastroenterology,
632 159 (2020) 388-390 e385.
633 [11] P. Shah, J.V. Fritz, E. Glaab, M.S. Desai, K. Greenhalgh, A. Frachet, M. Niegowska, M. Estes,
634 C. Jager, C. Seguin-Devaux, F. Zenhausern, P. Wilmes, A microfluidics-based in vitro model of
635 the gastrointestinal human-microbe interface, Nat Commun, 7 (2016) 11535.
636 [12] J. Zhang, Y.J. Huang, J.Y. Yoon, J. Kemmitt, C. Wright, K. Schneider, P. Sphabmixay, V.
637 Hernandez-Gordillo, S.J. Holcomb, B. Bhushan, G. Rohatgi, K. Benton, D. Carpenter, J.C. Kester,
638 G. Eng, D.T. Breault, O. Yilmaz, M. Taketani, C.A. Voigt, R.L. Carrier, D.L. Trumper, L.G.
639 Griffith, Primary human colonic mucosal barrier crosstalk with super oxygen-sensitive
640 Faecalibacterium prausnitzii in continuous culture, Med, 2 (2021) 74-98 e79.
641 [13] Y. Qi, L. Yu, F. Tian, J. Zhao, Q. Zhai, In vitro models to study human gut-microbiota
642 interactions: Applications, advances, and limitations, Microbiol Res, 270 (2023) 127336.
643 [14] Y. Sambuy, I. De Angelis, G. Ranaldi, M.L. Scarino, A. Stammati, F. Zucco, The Caco-2 cell
644 line as a model of the intestinal barrier: influence of cell and culture-related factors on Caco-2 cell
645 functional characteristics, Cell Biol Toxicol, 21 (2005) 1-26.

646 [15] X. Ding, X. Hu, Y. Chen, J. Xie, M. Ying, Y. Wang, Q. Yu, Differentiated Caco-2 cell models
647 in food-intestine interaction study: Current applications and future trends, Trends in Food
648 Science & Technology, 107 (2021) 455-465.
649 [16] G.P. Donaldson, S.M. Lee, S.K. Mazmanian, Gut biogeography of the bacterial microbiota,
650 Nat Rev Microbiol, 14 (2016) 20-32.
651 [17] T. Sato, D.E. Stange, M. Ferrante, R.G. Vries, J.H. Van Es, S. Van den Brink, W.J. Van Houdt,
652 A. Pronk, J. Van Gorp, P.D. Siersema, H. Clevers, Long-term expansion of epithelial organoids
653 from human colon, adenoma, adenocarcinoma, and Barrett's epithelium, Gastroenterology, 141
654 (2011) 1762-1772.
655 [18] T. Sato, R.G. Vries, H.J. Snippert, M. van de Wetering, N. Barker, D.E. Stange, J.H. van Es,
656 A. Abo, P. Kujala, P.J. Peters, H. Clevers, Single Lgr5 stem cells build crypt-villus structures in
657 vitro without a mesenchymal niche, Nature, 459 (2009) 262-265.
658 [19] Y. Wang, M. DiSalvo, D.B. Gunasekara, J. Dutton, A. Proctor, M.S. Lebhar, I.A. Williamson,
659 J. Speer, R.L. Howard, N.M. Smiddy, S.J. Bultman, C.E. Sims, S.T. Magness, N.L. Allbritton, Self-
660 renewing Monolayer of Primary Colonic or Rectal Epithelial Cells, Cell Mol Gastroenterol Hepatol,
661 4 (2017) 165-182 e167.
662 [20] M. Fujii, M. Matano, K. Toshimitsu, A. Takano, Y. Mikami, S. Nishikori, S. Sugimoto, T.
663 Sato, Human Intestinal Organoids Maintain Self-Renewal Capacity and Cellular Diversity in
664 Niche-Inspired Culture Condition, Cell Stem Cell, 23 (2018) 787-793 e786.
665 [21] C. Jumarie, C. Malo, Caco-2 cells cultured in serum-free medium as a model for the study of
666 enterocytic differentiation in vitro, J Cell Physiol, 149 (1991) 24-33.
667 [22] D. Mouradov, C. Sloggett, R.N. Jorissen, C.G. Love, S. Li, A.W. Burgess, D. Arango, R.L.
668 Strausberg, D. Buchanan, S. Wormald, L. O'Connor, J.L. Wilding, D. Bicknell, I.P. Tomlinson,
669 W.F. Bodmer, J.M. Mariadason, O.M. Sieber, Colorectal cancer cell lines are representative
670 models of the main molecular subtypes of primary cancer, Cancer Res, 74 (2014) 3238-3247.
671 [23] B.E. Michels, M.H. Mosa, B.M. Grebbin, D. Yepes, T. Darvishi, J. Hausmann, H. Urlaub, S.
672 Zeuzem, H.M. Kvasnicka, T. Oellerich, H.F. Farin, Human colon organoids reveal distinct
673 physiologic and oncogenic Wnt responses, J Exp Med, 216 (2019) 704-720.
674 [24] A. Niida, T. Hiroko, M. Kasai, Y. Furukawa, Y. Nakamura, Y. Suzuki, S. Sugano, T. Akiyama,
675 DKK1, a negative regulator of Wnt signaling, is a target of the beta-catenin/TCF pathway,
676 Oncogene, 23 (2004) 8520-8526.
677 [25] D. Yan, M. Wiesmann, M. Rohan, V. Chan, A.B. Jefferson, L. Guo, D. Sakamoto, R.H.
678 Caothien, J.H. Fuller, C. Reinhard, P.D. Garcia, F.M. Randazzo, J. Escobedo, W.J. Fantl, L.T.
679 Williams, Elevated expression of axin2 and hnkd mRNA provides evidence that Wnt/beta -catenin
680 signaling is activated in human colon tumors, Proc Natl Acad Sci U S A, 98 (2001) 14973-14978.
681 [26] J.F. Burgueno, M.T. Abreu, Epithelial Toll-like receptors and their role in gut homeostasis
682 and disease, Nat Rev Gastroenterol Hepatol, 17 (2020) 263-278.
683 [27] J.A. Hall, J.R. Grainger, S.P. Spencer, Y. Belkaid, The role of retinoic acid in tolerance and
684 immunity, Immunity, 35 (2011) 13-22.

685 [28] F.E. Johansen, C.S. Kaetzel, Regulation of the polymeric immunoglobulin receptor and IgA
686 transport: new advances in environmental factors that stimulate pIgR expression and its role in
687 mucosal immunity, Mucosal Immunol, 4 (2011) 598-602.
688 [29] R. McCoy, S. Oldroyd, W. Yang, K. Wang, D. Hoven, D. Bulmer, M. Zilbauer, R.M. Owens,
689 In Vitro Models for Investigating Intestinal Host-Pathogen Interactions, Adv Sci (Weinh), 11
690 (2024) e2306727.
691 [30] M. Derrien, F. Turroni, M. Ventura, D. van Sinderen, Insights into endogenous
692 Bifidobacterium species in the human gut microbiota during adulthood, Trends Microbiol, 30
693 (2022) 940-947.
694 [31] Y. Luo, C. Xie, C.N. Brocker, J. Fan, X. Wu, L. Feng, Q. Wang, J. Zhao, D. Lu, M. Tandon,
695 M. Cam, K.W. Krausz, W. Liu, F.J. Gonzalez, Intestinal PPARalpha Protects Against Colon
696 Carcinogenesis via Regulation of Methyltransferases DNMT1 and PRMT6, Gastroenterology, 157
697 (2019) 744-759 e744.
698 [32] S. Kersten, S. Mandard, N.S. Tan, P. Escher, D. Metzger, P. Chambon, F.J. Gonzalez, B.
699 Desvergne, W. Wahli, Characterization of the fasting-induced adipose factor FIAF, a novel
700 peroxisome proliferator-activated receptor target gene, J Biol Chem, 275 (2000) 28488-28493.
701 [33] M.M. Rahman, G. McFadden, Modulation of NF-kappaB signalling by microbial pathogens,
702 Nat Rev Microbiol, 9 (2011) 291-306.
703 [34] M. Friedrich, M. Pohin, F. Powrie, Cytokine Networks in the Pathophysiology of
704 Inflammatory Bowel Disease, Immunity, 50 (2019) 992-1006.
705 [35] G.D. Bren, N.J. Solan, H. Miyoshi, K.N. Pennington, L.J. Pobst, C.V. Paya, Transcription of
706 the RelB gene is regulated by NF-kappaB, Oncogene, 20 (2001) 7722-7733.
707 [36] A. Mantovani, C.A. Dinarello, M. Molgora, C. Garlanda, Interleukin-1 and Related Cytokines
708 in the Regulation of Inflammation and Immunity, Immunity, 50 (2019) 778-795.
709 [37] M.A. McGuckin, R. Eri, L.A. Simms, T.H. Florin, G. Radford-Smith, Intestinal barrier
710 dysfunction in inflammatory bowel diseases, Inflamm Bowel Dis, 15 (2009) 100-113.
711 [38] E.E. Marr, T.J. Mulhern, M. Welch, P. Keegan, C. Caballero-Franco, B.G. Johnson, M.
712 Kasaian, H. Azizgolshani, T. Petrie, J. Charest, E. Wiellette, A platform to reproducibly evaluate
713 human colon permeability and damage, Sci Rep, 13 (2023) 8922.
714 [39] K. Kulthong, G. Hooiveld, L. Duivenvoorde, I. Miro Estruch, V. Marin, M. van der Zande, H.
715 Bouwmeester, Transcriptome comparisons of in vitro intestinal epithelia grown under static and
716 microfluidic gut-on-chip conditions with in vivo human epithelia, Sci Rep, 11 (2021) 3234.
717 [40] D. Cheng, M.Z. Xie, A review of a potential and promising probiotic candidate-Akkermansia
718 muciniphila, J Appl Microbiol, 130 (2021) 1813-1822.
719 [41] N. Panse, P.M. Gerk, The Caco-2 Model: Modifications and enhancements to improve
720 efficiency and predictive performance, Int J Pharm, 624 (2022) 122004.
721 [42] R.G. Bristow, R.P. Hill, Hypoxia and metabolism. Hypoxia, DNA repair and genetic
722 instability, Nat Rev Cancer, 8 (2008) 180-192.
723 [43] E.K. Mallott, K.R. Amato, Host specificity of the gut microbiome, Nat Rev Microbiol, 19

(2021) 639-653.
[44] M. Sadaghian Sadabad, J.Z. von Martels, M.T. Khan, T. Blokzijl, G. Paglia, G. Dijkstra, H.J. Harmsen, K.N. Faber, A simple coculture system shows mutualism between anaerobic faecalibacteria and epithelial Caco-2 cells, Sci Rep, 5 (2015) 17906.
[45] J.M. Allaire, S.M. Crowley, H.T. Law, S.Y. Chang, H.J. Ko, B.A. Vallance, The Intestinal Epithelium: Central Coordinator of Mucosal Immunity, Trends Immunol, 39 (2018) 677-696.
[46] R. Abdulqadir, J. Engers, R. Al-Sadi, Role of Bifidobacterium in Modulating the Intestinal Epithelial Tight Junction Barrier: Current Knowledge and Perspectives, Curr Dev Nutr, 7 (2023) 102026.
[47] M.A. Garcia, W.J. Nelson, N. Chavez, Cell-Cell Junctions Organize Structural and Signaling Networks, Cold Spring Harb Perspect Biol, 10 (2018).
[48] X. Shu, J. Wang, L. Zhao, J. Wang, P. Wang, F. Zhang, R. Wang, Bifidobacterium lactis TY-S01 protects against alcoholic liver injury in mice by regulating intestinal barrier function and gut microbiota, Heliyon, 9 (2023) e17878.
[49] K.R. Bergmann, S.X. Liu, R. Tian, A. Kushnir, J.R. Turner, H.L. Li, P.M. Chou, C.R. Weber, I.G. De Plaen, Bifidobacteria stabilize claudins at tight junctions and prevent intestinal barrier dysfunction in mouse necrotizing enterocolitis, Am J Pathol, 182 (2013) 1595-1606.
[50] A. Horowitz, S.D. Chanez-Paredes, X. Haest, J.R. Turner, Paracellular permeability and tight junction regulation in gut health and disease, Nat Rev Gastroenterol Hepatol, 20 (2023) 417-432.
[51] S. Prasad, R. Mingrino, K. Kaukinen, K.L. Hayes, R.M. Powell, T.T. MacDonald, J.E. Collins, Inflammatory processes have differential effects on claudins 2, 3 and 4 in colonic epithelial cells, Lab Invest, 85 (2005) 1139-1162.
[52] S. Zeissig, N. Burgel, D. Gunzel, J. Richter, J. Mankertz, U. Wahnschaffe, A.J. Kroesen, M. Zeitz, M. Fromm, J.D. Schulzke, Changes in expression and distribution of claudin 2, 5 and 8 lead to discontinuous tight junctions and barrier dysfunction in active Crohn's disease, Gut, 56 (2007) 61-72.
[53] T. Oshima, H. Miwa, T. Joh, Changes in the expression of claudins in active ulcerative colitis, J Gastroenterol Hepatol, 23 Suppl 2 (2008) S146-150.
[54] L. Ding, Z. Lu, O. Foreman, R. Tatum, Q. Lu, R. Renegar, J. Cao, Y.H. Chen, Inflammation and disruption of the mucosal architecture in claudin-7-deficient mice, Gastroenterology, 142 (2012) 305-315.
[55] J. Stutzmann, A. Bellissent-Waydelich, L. Fontao, J.F. Launay, P. Simon-Assmann, Adhesion complexes implicated in intestinal epithelial cell-matrix interactions, Microsc Res Tech, 51 (2000) 179-190.
[56] D. Kim, J.M. Paggi, C. Park, C. Bennett, S.L. Salzberg, Graph-based genome alignment and genotyping with HISAT2 and HISAT-genotype, Nat Biotechnol, 37 (2019) 907-915.
[57] M. Pertea, G.M. Pertea, C.M. Antonescu, T.C. Chang, J.T. Mendell, S.L. Salzberg, StringTie enables improved reconstruction of a transcriptome from RNA-seq reads, Nat Biotechnol, 33 (2015) 290-295.

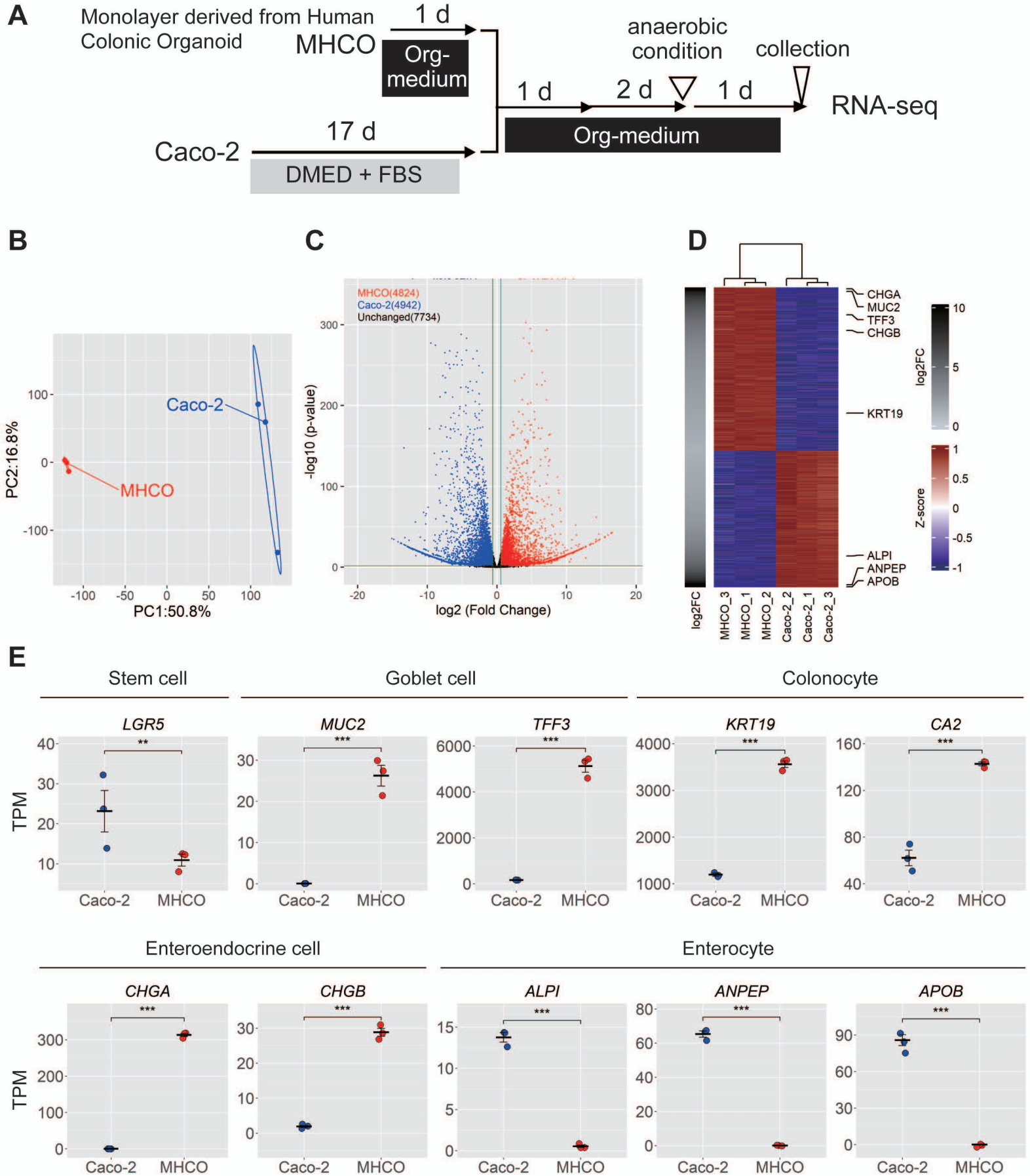

Figure 1. Sen et al.

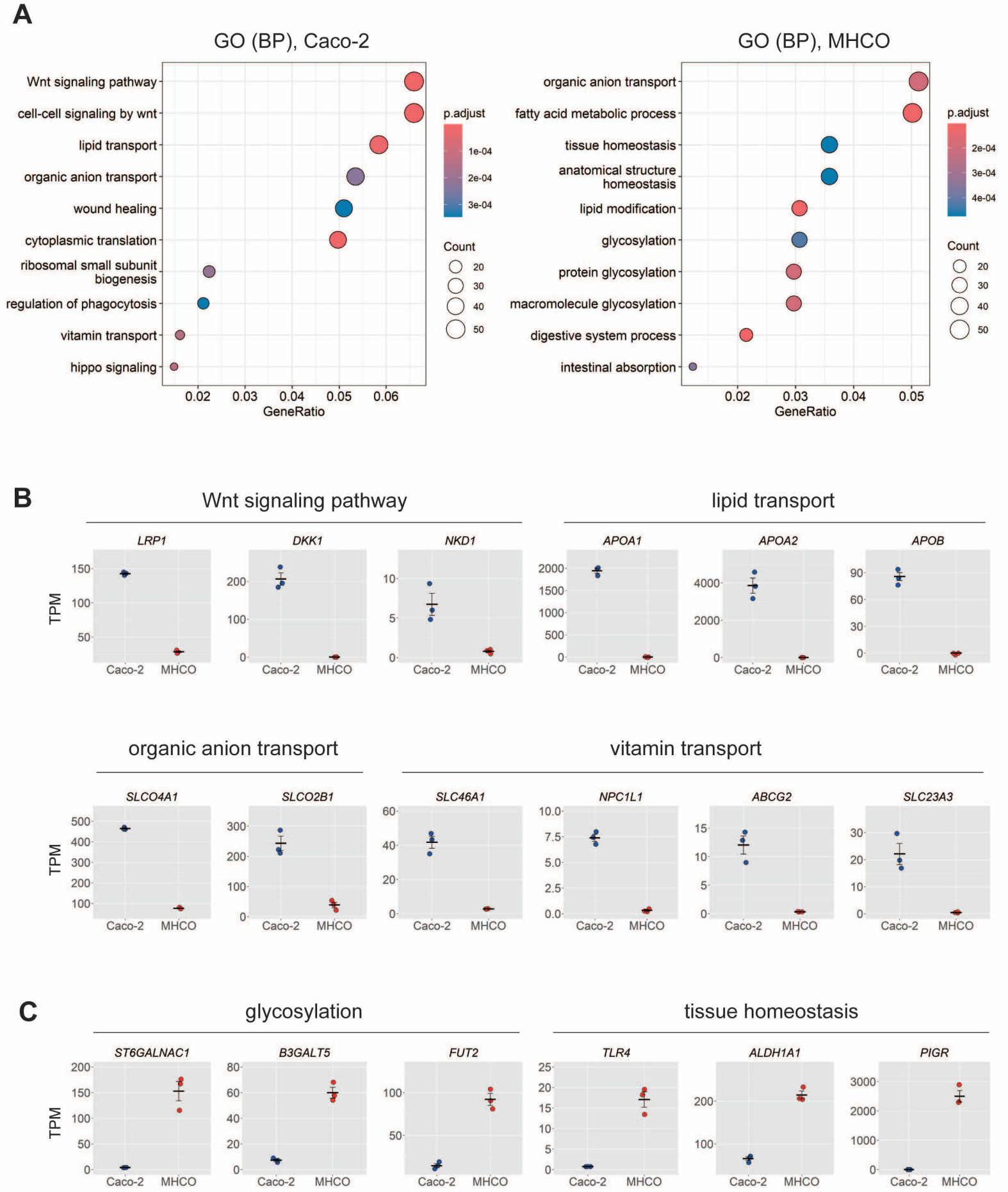

Figure 2. Sen et al.

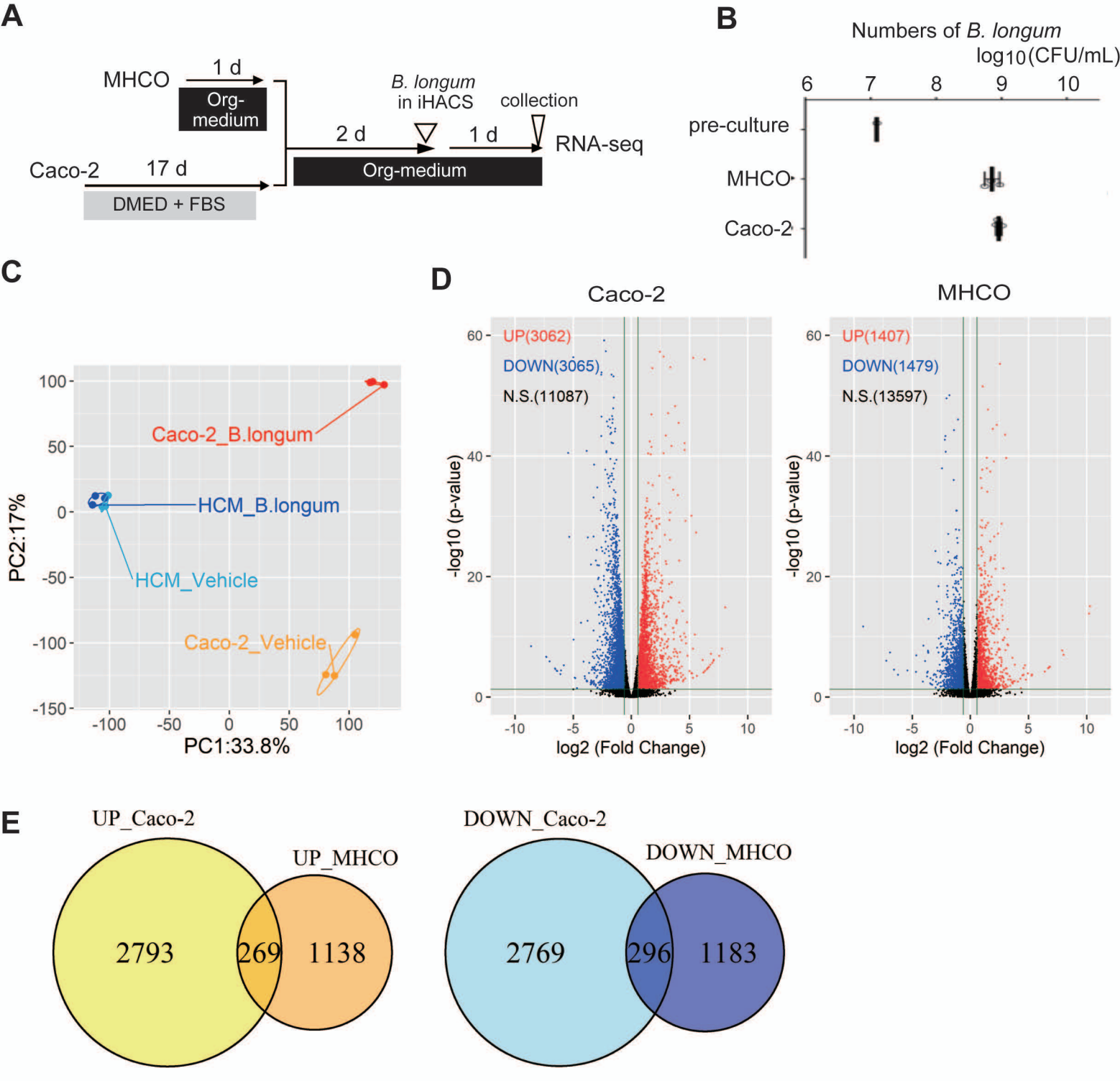

Figure 3. Sen et al.

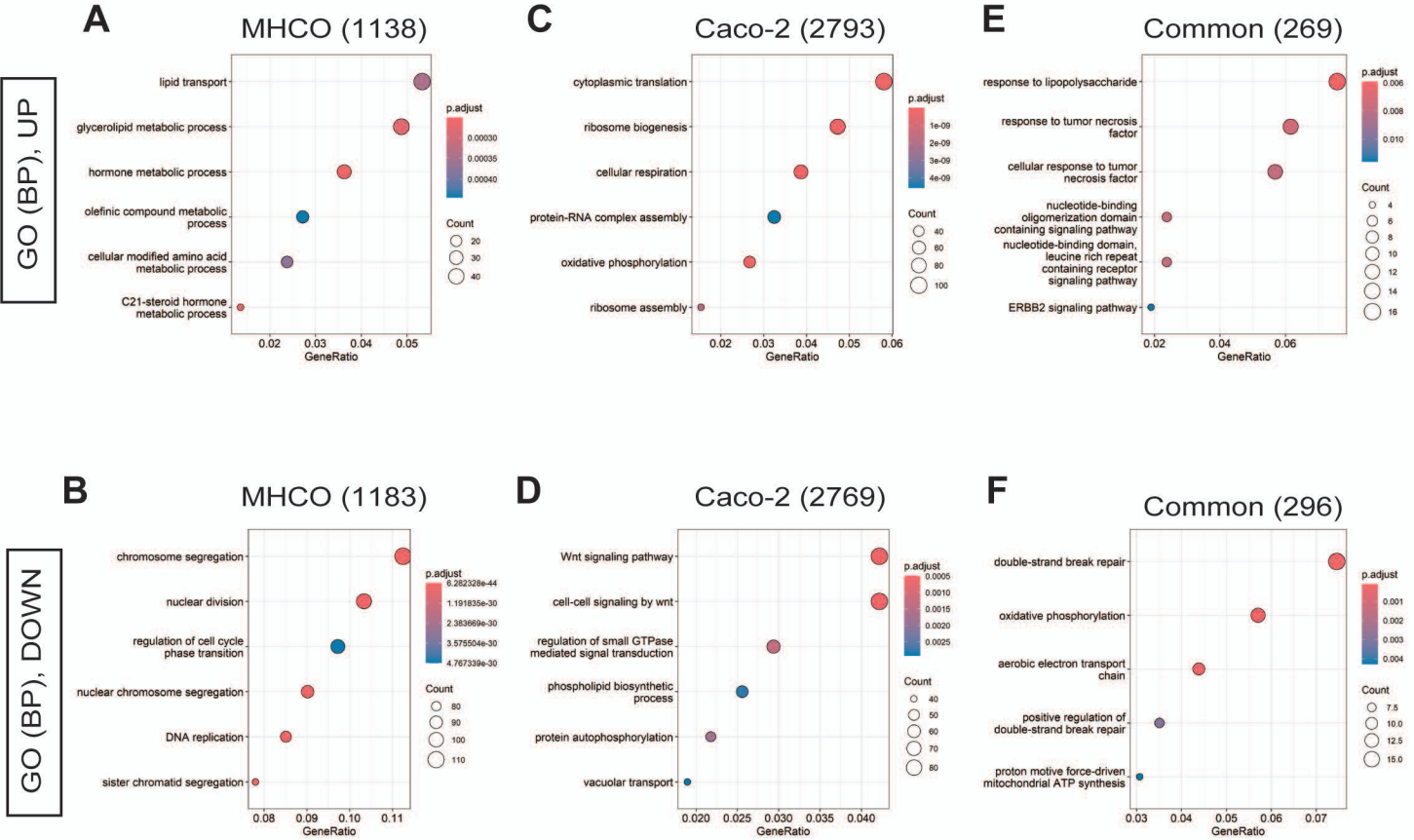

Figure 4. Sen et al.

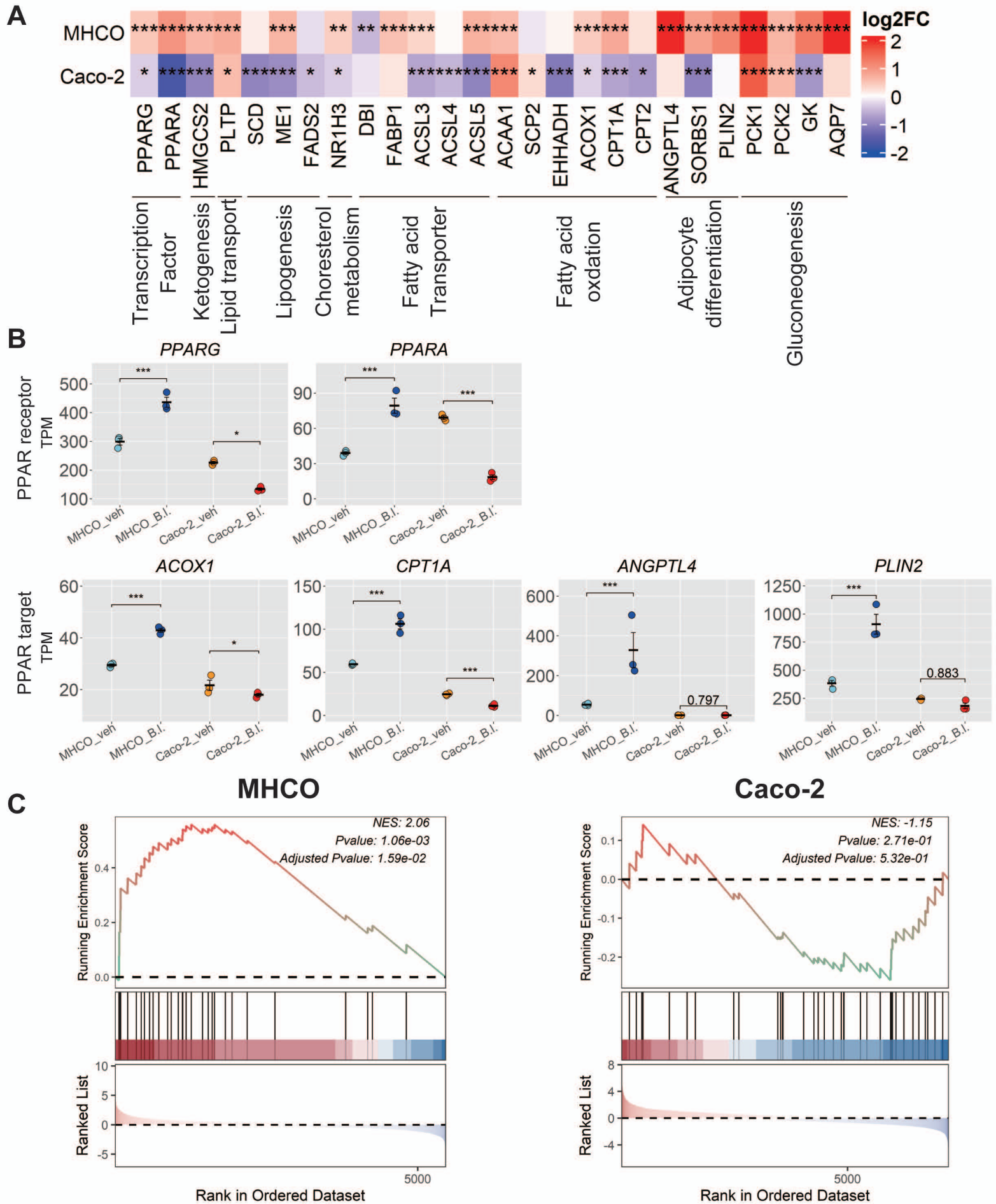

Figure 5. Sen et al.

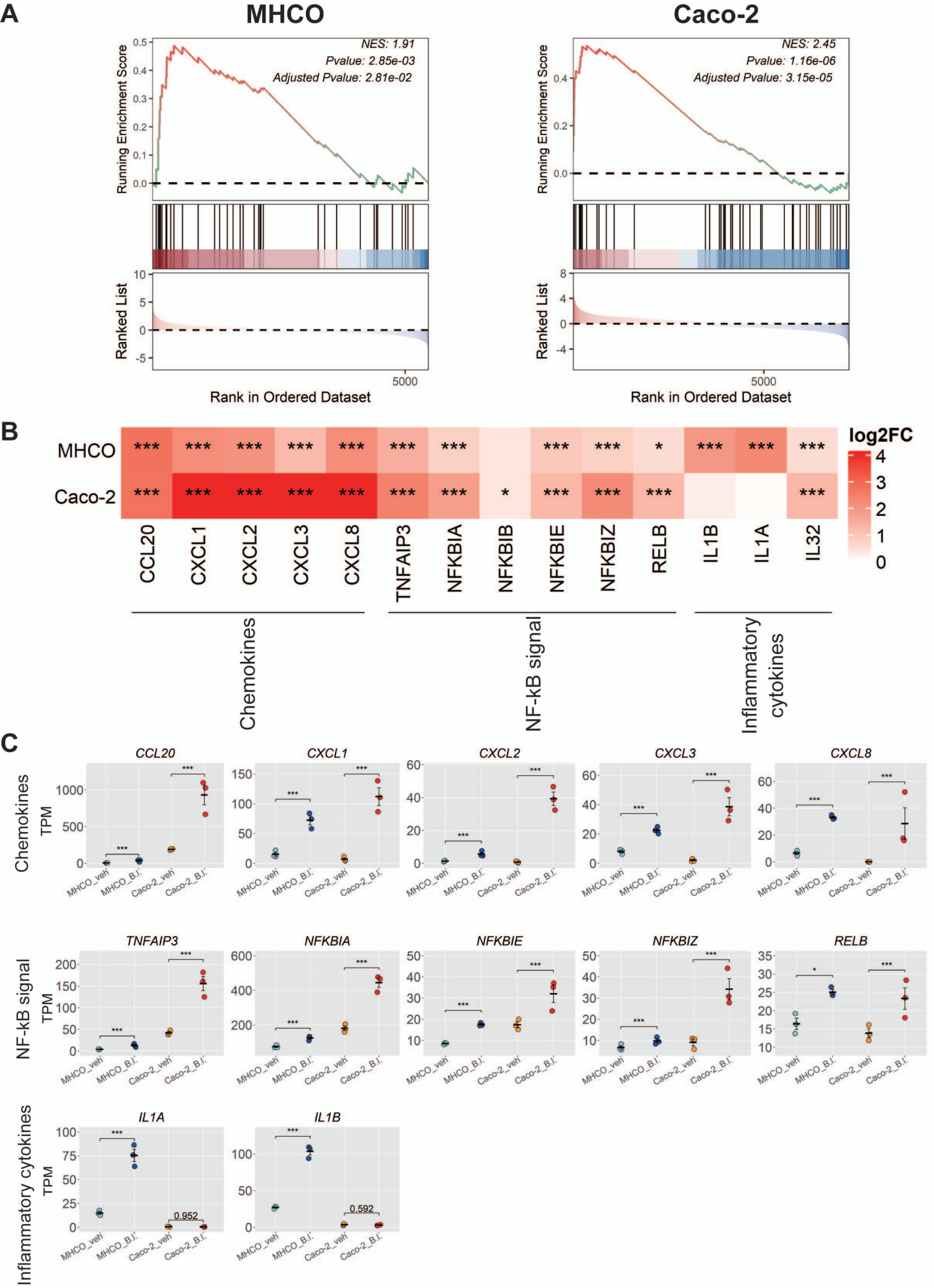

Figure 6. Sen et al.

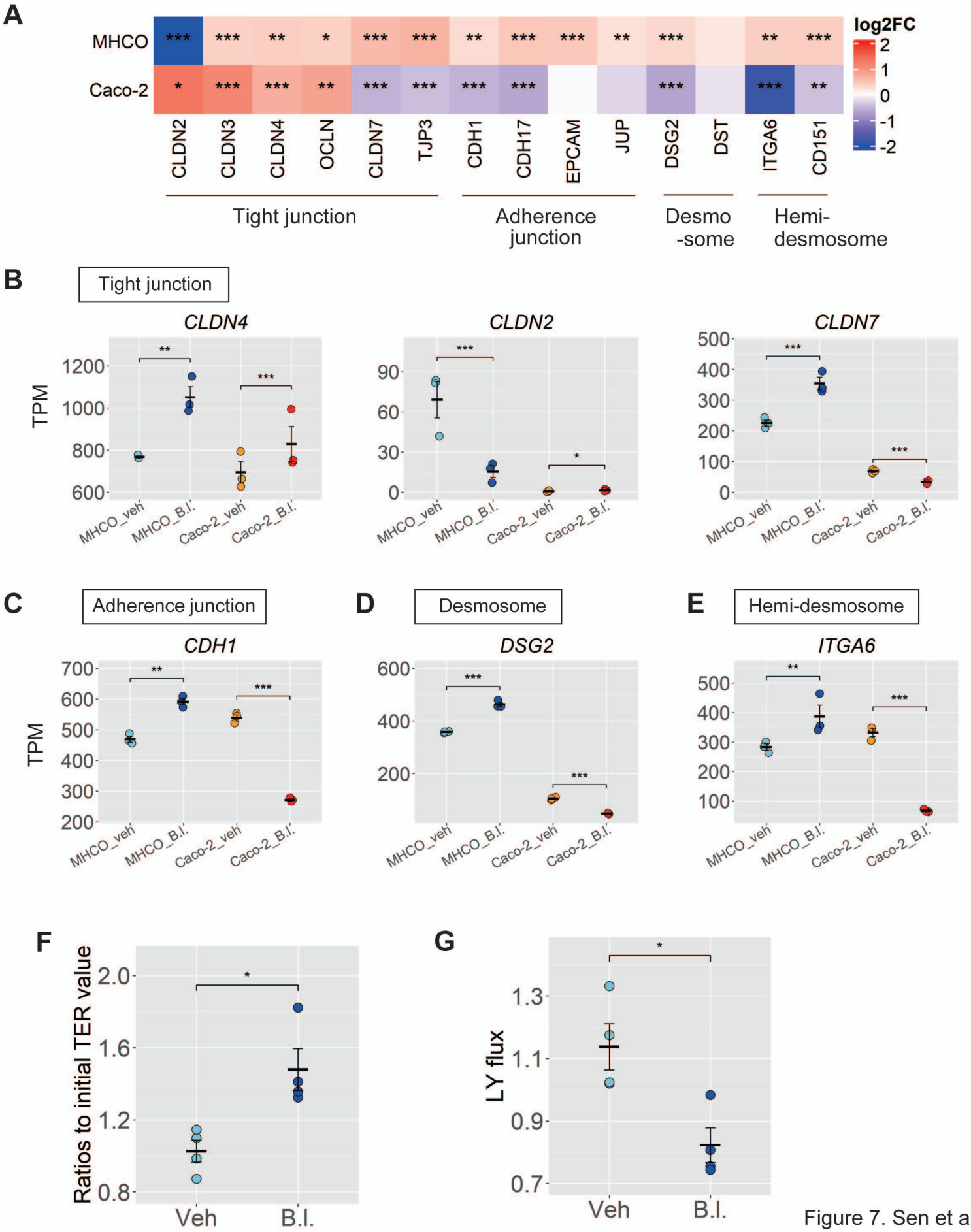

Figure 7. Sen et al.